Resolving decay-time dependent photoluminescence induced by phonon-dressed excitons in ZnO

Ryu Yukawa,[1,2,*] Susumu Yamamoto,[2,3,4] Ren Arita,[5] Yuki Minami,[5] Kohei Yamanoi,[5] Kenichi Ozawa,[6,7]
Kazuyuki Sakamoto,[1,8,9] Toshihiko Shimizu,[5] Nobuhiko Sarukura,[5] and Iwao Matsuda[2,10]
[1]Department of Applied Physics, Osaka University, Suita, Osaka 565-0871, Japan
[2]Institute for Solid State Physics, The University of Tokyo, Kashiwa, Chiba 277-8581, Japan
[3]International Center for Synchrotron Radiation Innovation Smart (SRIS), Tohoku University, Sendai, Miyagi 980-8577, Japan
[4]Institute of Multidisciplinary Research for Advanced Materials (IMRAM), Tohoku University, Sendai, Miyagi 980-8577, Japan
[5]Institute of Laser Engineering, Osaka University, Suita, Osaka 565-0871, Japan
[6]Institute of Materials Structure Science, High Energy Accelerator Research Organization (KEK), Tsukuba, Ibaraki 305-0801, Japan
[7]SOKENDAI (The Graduate University for Advanced Studies), Tsukuba, Ibaraki 305-0801, Japan
[8]Center for Spintronics Research Network, Graduate School of Engineering Science, Osaka University, Toyonaka, Osaka 560-8531, Japan
[9]Spintronics Research Network Division, Institute for Open and Transdisciplinary Research Initiatives,
Osaka University, Suita, Osaka 565-0871, Japan
[10]Trans-scale Quantum Science Institute, The University of Tokyo, Bunkyo, Tokyo 113-0033, Japan

(Received 2 September 2021; revised 2 August 2022; accepted 19 September 2022; published 21 October 2022)

Time-resolved photoluminescence (PL) experiments on ZnO crystals have been conducted at room temperature to elucidate the origins of a near-band edge (NBE) emission. A temporal profile of the PL spectra exhibits a two-curve structure with different decaying rates and is reproduced reasonably by a biexponential function, indicating that there are at least two origins with different decay times in the NBE emission. By taking free exciton (FX)–longitudinal optical (LO) phonon interactions into account in the analysis of the PL spectra, the faster and slower decaying emissions are found to be associated with stronger and weaker FX-LO phonon coupling, respectively. We propose that the NBE emissions with different decay times are related to crystal imperfections; the fast-decaying emission originates from the region with a higher density of defects or impurities, while the slower one is from the regions with better crystallinity.

DOI: 10.1103/PhysRevMaterials.6.104607

I. INTRODUCTION

Zinc oxide (ZnO) is a transparent semiconductor crystal with a wide band gap E_g of 3.37 eV at room temperature [1]. It has attracted huge attention for its optoelectronic applications, such as blue and ultraviolet (UV) light-emitting diodes [2,3] and fast extreme UV scintillators [4]. Under an ambient condition, recombination of a loosely bound electron (*e*) and hole (*h*) pair, i.e., a free exciton (FX), contributes to the photoluminescence (PL) in the UV energy range. Since the binding energy of the FX is 60 meV [1,5] and exceeds the thermal energy at room temperature, the dynamical behavior of FXs governs the PL process and thus controls the performance of optoelectronic devices [6–8]. The FX dynamics have been experimentally examined by probing temporal variations of the PL using the pump-probe method [6,9–12]. The dynamics are basically described as a sequence of (i) interband excitation of electrons over the ZnO band gap by a femtosecond optical pulse, (ii) formation of FXs within a few picoseconds [13], and (iii) generation of PL by the *e-h* recombination. The PL energy of ZnO, ∼3.3 eV, agrees with the difference between the ZnO band-gap energy and the FX binding energy, and thus, this PL is often called a near-band edge (NBE) emission [Fig. 1(a)].

The lifetime of the FX through the direct recombination, obtained in NBE emission in a high purity ZnO crystal, is longer than 10 ns [14] due to the large binding energy of the FX. However, it has been reported that the PL process is mostly completed in much shorter times (<1 ns), indicating that PL process consists of several recombination origins that shorten the decay times [6,9–12]. These PL origins can be classified into two groups depending on the decay times: one has a time scale of 10–100 ps and the other has slower decay times with 100–1000 ps. This means that despite the simple picture of the NBE emission [Fig. 1(a)], the relaxation process of the photoexcited electrons is rather complicated and should consist of multipath dynamics involving external factors, such as crystal imperfections caused by impurities and defects in the ZnO samples. As for the recombination processes that are induced by impurity and/or defect states, the relaxation processes associated with orange (1.9 eV) or green (2.4 eV) light emissions have been reported [15,16]. In addition, the processes without emitting photons in the visible light range have been reported [9,17] and are termed nonradiative recombination processes. In an ordinary ZnO crystal with some impurities and defects, recombination processes through the nonradiative channels are much faster than the direct recombination process. Thus, the depopulation rates

*ryukawa@ap.eng.osaka-u.ac.jp

 ©2022 American Physical Society

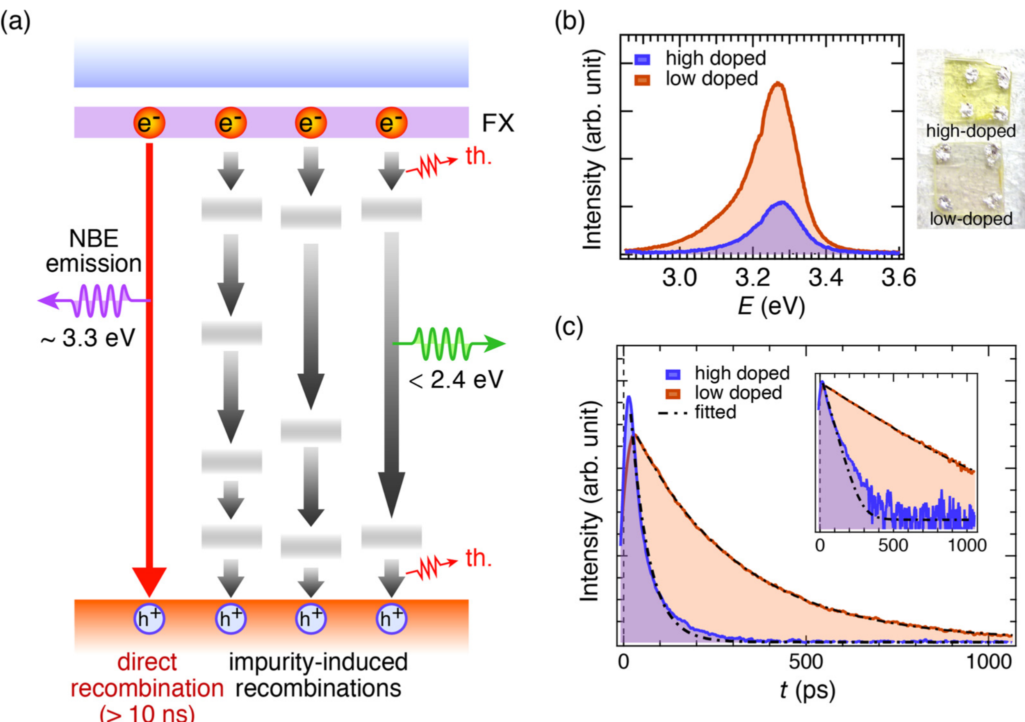

FIG. 1. (a) Schematic image for the NBE emission (red arrow) in ZnO and examples of impurity-induced recombinations that do not involve the NBE emission (black arrows). The top blue area and the bottom orange area represent the conduction band and valence band, respectively. In the direct recombination processes, an electron in the FX level directly drops to the valence band and recombines with a hole while emitting an NBE light (energy of about 3.3 eV). In the impurity-induced recombination processes, an electron in the FX level or conduction band drops to the valence band via the impurity and/or defect states (shaded in gray) and finally recombines with a hole. During the relaxation processes, energies are transferred to heats and/or lights with smaller energy (~2.4 eV or lower) than the NBE emission energy. In a doped crystal, a decay time of NBE PL, i.e. a lifetime of excited electrons in the FX level, depends on the density of the impurity-induced recombination channels. (b),(c) Time-integrated (b) and energy-integrated (c) PL intensity profiles of the NBE emissions taken for the high-doped (blue curves) and low-doped (orange curves) ZnO crystals. The energy-integrated PL intensity profiles are also displayed logarithmically in the inset of (c). The same laser intensity of 1.7 mJ/cm^2/pulse with the wavelength of 290 nm was used for the excitation of electrons in both the ZnO crystals. The decay profiles for the high-doped and low-doped ZnO are fitted by single-exponential functions (dashed curves) with lifetimes of 50 ps and 290 ps, respectively. The photograph taken for the high-doped (upper) and low-doped (lower) ZnO crystals used for the PL experiments and Hall measurements is shown on the right side of (b). Here, the samples are placed on pulp paper, and the four metallic points seen on each sample have been used for the Hall measurements.

of the photoexcited carriers (the decay times of the NBE PL) have been discussed in terms of the *e*-*h* recombination through impurity and/or defect levels within the band gap [17] [Fig. 1(a)]. Despite tremendous efforts by preceding studies, a proper understanding of the extrinsic channels during the PL process and their influences on the FX dynamics has not yet been established. One reason is that most of the previous studies have mainly discussed the origin of the NBE PL from decay curves of the energy-integrated PL spectra where important information about the FX-phonon interaction is smeared out. Therefore, incorporating FX-phonon interactions, which have been employed in the analysis of static NBE PL spectra [5,6,18–21], into the analysis of the time evolution of NBE PL spectra is expected to provide deeper insight into the origin of the NBE emission.

In this study, we performed time-resolved experiments in picosecond order to investigate the NBE PL process of ZnO. Two ZnO crystals with different impurity concentrations were examined. The NBE PL intensity decay was found to be faster for the ZnO crystal with high impurities than that with low impurities, indicating that the fast process is more sensitive to the impurity concentrations. The spectral analysis of the decaying process further revealed that the appearance of PL processes with different decay times is due to the nonuniform distribution of impurities. These results indicate that the spatial distribution of the sites where the impurity-induced fast *e*-*h* recombination is enhanced must be taken into account to grasp the whole picture of the FX dynamics and to control the PL decay time in ZnO.

II. EXPERIMENT

All the experiments were conducted at room temperature under an atmosphere condition. The PL light was measured by a synchroscan streak unit (Hamamatsu M1955). To excite electrons over the band gap of ZnO, laser light with a wavelength (photon energy) of 290 nm (4.28 eV) was generated by the third harmonics of a mode-locked Ti:sapphire laser, and its intensity was set at 1.7 mJ/cm^2/pulse during the experiments. The total energy and temporal resolutions

of the optical detector in the present experimental setup were 92 meV and 30 ps, respectively (see Note 1 in the Supplemental Material [22] for more details about the energy and temporal resolutions). Two ZnO wafers with different amounts of doping were measured: a high-doped ZnO (Goodwill, Russia) and a low-doped one (MTI Corp., U.S.). The concentrations of the carriers (electrons), which result from the presence of impurities and/or defects, were determined by the Hall measurements to be 1.9×10^{14} cm^{-3} and 3.4×10^{13} cm^{-3} for the high- and low-doped samples, respectively.

III. RESULTS AND DISCUSSION

The intensity profiles of time-integrated PL spectra of the high- and low-doped ZnO crystals are shown in Fig. 1(b). Both spectra exhibit peaks at around 3.3 eV, which corresponds to the direct recombination process of the FX. On the other hand, the temporal profiles of the PL intensity contrast distinctly with each other, as presented in Fig. 1(c). The intensity decay completes at around 300 ps for the high-doped sample, while the decay continues even at 1000 ps (1 ns) for the low-doped one. Since the intrinsic lifetime of the FX is longer than 10 ns in ZnO [14], these results indicate that the FX lifetime is shortened in both the ZnO samples with a greater extent for the ZnO crystal with the higher impurity concentration. As illustrated in Fig. 1(a), the doped ZnO crystal would promote *e-h* recombination due to an increase in the number of recombination channels that do not accompany the NBE emission. Thus, an increase in the impurity concentration shortens the FX lifetime (i.e., the depopulation rate of excited electrons in the FX level). This explanation is supported by the difference in the PL intensity between the high- and low-doped ZnO [Fig. 1(b)]; reflecting larger number of the impurity-induced recombination channels that do not contribute to the NBE emission, the NBE PL intensity of the high-doped ZnO sample is weaker than that of the low-doped one.

To unveil details of the relaxation process, we analyzed the temporal variation of the PL intensity quantitatively by analytical functions. Figure 1(c) shows the least-square fitting results of the PL intensity profiles by a single exponential function. The time dependence of the PL intensity of the low-doped sample is well fitted to a single exponential function with a lifetime of 290 ps, whereas that of the high-doped sample is not fitted properly (see also Note 3 in the Supplemental Material [22] about the fitting results for the PL intensity of the low-doped sample). The intensity decay in the high-doped one is quite complicated as demonstrated in Fig. 2. Figure 2(a) shows the energy and temporal (E-t) diagram of the PL intensity for the high-doped ZnO crystal. The intensity peak is located at around 3.26 eV, and the intensity steeply drops at both energy sides. At all energies, a decay of the intensity with time is observed. Notably, the intensity drops rapidly below 50 ps and then decays at a relatively slow rate. The dynamical properties appear in detail when the PL intensities are plotted logarithmically, as shown in Fig. 2(b) for emissions in the energy range 3.04–3.36 eV. Here, the shape of the decay curve is found to change by energy; a bending feature is visible at around 60 ps for $E = 3.36$ eV and $E < 3.12$ eV, but not clearly seen at around 3.28 eV (see also Note 2 in the

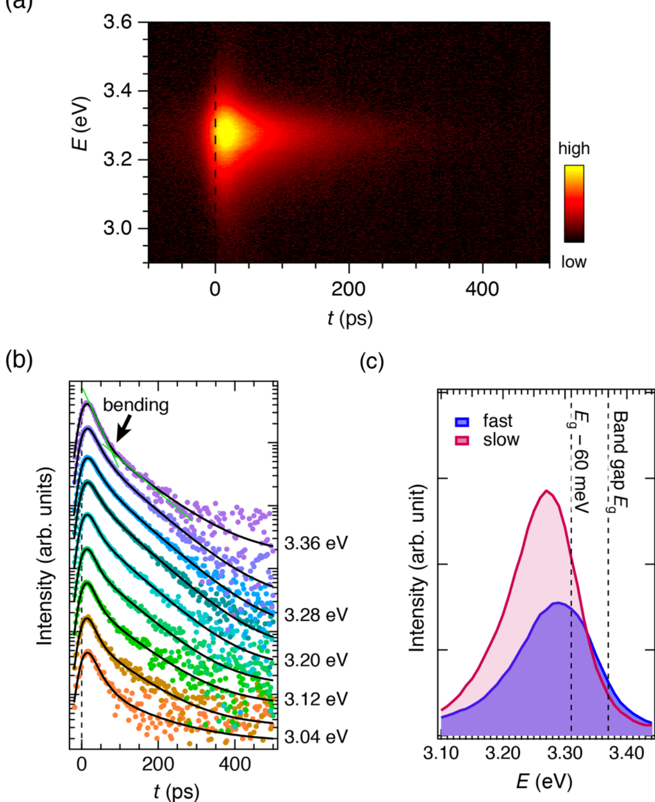

FIG. 2. (a) Time- and energy-resolved PL intensity map taken for the high-doped ZnO which was irradiated with a laser of the intensity of 1.7 mJ/cm^2/pulse. Its temporal profiles extracted in the energy range 3.04–3.36 eV with the interval of 0.04 eV are logarithmically displayed in (b). Here, in order to make the comparison of the spectral shapes clearer, the temporal profiles are displayed with intensity offsets. The green lines shown on the temporal profile at 3.36 eV are the guide for the eye to make a bending feature clearer. The curve fitting results are overlaid with the black curves. (c) Time-integrated PL intensity profiles of the fast and slow decays [$I_f(E)\tau_f(E)$ and $I_s(E)\tau_s(E)$].

Supplemental Material [22] for more details about the shape of the decay curves). Thus, under the assumption that two different PL origins contribute to the PL, the time-resolved intensity $I(E, t)$ was fitted by two exponential functions with a fast decay constant $\tau_f(E)$ and a slow decay constant $\tau_s(E)$:

$$I(E, t) = \Theta(t)\left\{I_f(E)\exp\left(-\frac{t}{\tau_f(E)}\right) + I_s(E)\exp\left(-\frac{t}{\tau_s(E)}\right)\right\} + I_{B.G.}, \quad (1)$$

where $I_f(E)$ and $I_s(E)$ are the PL intensities at $t = 0$ for the fast and slow decay processes, respectively, $I_{B.G.}$ is the intensity of the constant background, and $\Theta(t)$ is the unit step function: $\Theta(t) = 1$ for $t \geqslant 0$ and 0 otherwise. The function is an extension of the intensities and lifetimes of the biexponential decay function [6,7,9,14] to be the energy-dependent values. The time-dependent PL intensities were fitted by the least square method using Eq. (1) with a convolution of a Gaussian function whose full width at half maximum

(FWHM) was set to the experimental resolution, 33 ps. Fitted curves reproduce well the experimental decay curves as shown in Fig. 2(b). The lifetimes are nearly independent of the PL energy to be $\tau_f \sim 20$ ps and $\tau_s \sim 80$ ps near the PL peak (3.1 eV $< E <$ 3.4 eV) (see also Note 2 in the Supplemental Material [22] for more details about the obtained decay constants). Thus, the energy dependence of the decay profile is essentially attributed to the difference between the $I_f(E)$ and $I_s(E)$ contributions. The spectral shapes and intensities between the fast and slow decays are compared in Fig. 2(c), where time-integrated PL spectra, $I_f(E)\tau_f(E)$ and $I_s(E)\tau_s(E)$, are displayed. The integrated intensity of the slowly decaying emission is about 1.6 times larger than that of the fast process. Recalling the NBE emission process [Fig. 1(a)], the slower and faster decay components should originate from a region with the lower and higher impurity/defect concentration, respectively.

A closer look at Fig. 2(c) shows that the energy positions of the PL peaks differ from each other by 25 meV and both are lower than the FX level ($E_g - 60$ meV $\sim$ 3.31 eV). One may think that the origin of the peak shifts is due to the possible band-gap reduction induced by the laser heating effect. However, considering that the thermal effect should also lead to a broadening of the spectral width [6], a narrower width for the slow decay (0.13 eV) than the fast one (0.15 eV) negates this effect. Another plausible origin is a contribution of a donor-bound exciton, another major exciton. However, this is also negated because the PL from the donor-bound exciton state is observed only at low temperatures ($<$160 K) [6]. As judged from the energy scale, interactions between the excitons and longitudinal optical (LO) phonons are the most plausible origin of the peak shifts. Actually, it has been widely known from preceding static PL studies that electrons as well as FXs in a ZnO crystal can couple with LO phonons due to the high polarity of the material [8,18,23,24] and that the FX emission at room temperature fundamentally involves the LO phonon excitations [5,6,8,18,24]. Thus, the FX-LO phonon interactions are essential to explain the differences in the spectral shapes.

The PL spectra in Fig. 2(c) extend a rather wide energy range between 3.10 and 3.40 eV. Because the LO phonon energy is only 72 meV, energy loss processes with multiple LO phonon excitations must be considered to explain the spectral shapes. In the processes, the energy intervals of the multiple LO phonon excitations correspond to the excitation energy of an LO phonon [$\hbar\omega_{LO} =$ 72 meV (Ref. [25])]. In addition, the intensity of the multiple LO phonon excitation (I_n; $n \geqslant 1$ is the number of LO phonon excitation) is required to follow the relation [7,19,20,24,26]

$$I_n = \left(\frac{S}{n}\right) I_{n-1}, \quad (2)$$

where S is the Huang-Rhys factor that determines the mean number of created phonons and is, thus, related to the exciton-LO phonon coupling strength [7,20,26]. Using Eq. (2), the PL profiles of the fast and slow processes were analyzed by a least-square fitting. For simplicity, the fitting was made by assuming that all the peaks were represented by a Gaussian function with an energy interval of $\hbar\omega_{LO}$. Furthermore, due to the thermal excitations, the peak position of the FX emission is set to be shifted upward in $\frac{3}{2}k_BT$ from $E_g - 60$ meV [6]. Here, k_B is the Boltzmann constant and T is the temperature. It should be noted that the most accepted value of the band gap ($E_g = 3.37$ eV) is used for the fitting of the intensity profiles. The same conclusion can be obtained even if the actual value of the band gap deviates from the 3.37 eV (see Note 4 in the Supplemental Material [22] for more details about the fitting conditions). The fitting results for $I_f(E)$ and $I_s(E)$ are displayed in Fig. 3(a), where the spectra are normalized to their peak heights for a clear comparison of the spectral shapes. It should be noted that since τ_f and τ_s in Eq. (1) are almost energy invariant, the spectral shapes of the fast and slow decays displayed in Fig. 3(a) are identical to the ones shown in Fig. 2(c). The fitting results show that the energy position of the single LO phonon emission locates near the spectral peaks and the multiple LO phonon excitations form the tail structures at the low energy sides. These features are identical to the analysis results of static PL spectra reported previously [5,6,21]. Furthermore, the Gaussian width (FWHM $\sim$ 100 meV) obtained from the fittings is in reasonable agreement with the value shown in the previous study ($\sim$ 80 meV) [21]. These agreements indicate that the analytical method that has been used for the static PL spectra is also applied to the time-resolved PL spectra of ZnO to understand the FX-LO phonon interactions and enables us to compare the FX-LO phonon coupling strength between the fast and slow decays.

Both fitting results shown in Fig. 3(a) have the similarity that the intensity of the 1-LO phonon-derived peak (I_1) at $E \sim 3.28$ eV is larger than that of the FX peak (I_0) at $E \sim 3.35$ eV. The differences in the spectral shapes of $I_f(E)$ and $I_s(E)$ mainly originate from the relative intensities of I_0/I_1 and attenuation rates (S/n) of the LO peaks for $n \geqslant 1$. The intensity ratio for $I_f(E)(I_0/I_1 = 0.59)$ is much larger than that for $I_s(E)(I_0/I_1 = 0.05)$, while the attenuation rate for $I_f(E)$ is smaller than that for $I_s(E)$. The latter difference results from the fact that the S value for $I_f(E)$ ($S = 1.00$) is larger than that for $I_s(E)$ ($S = 0.74$), resulting in the weaker attenuation of the tail structure for $I_f(E)$. The obtained S values are in reasonable agreement with those reported previously [$S = 0.64$–1.4 (Refs. [21,24])] and the quantitative difference in S between the fast and slow processes can consistently be understood in terms of the impurity-induced recombination process. It has been known that the FX couples more strongly to LO phonons (S value increases) when the impurity concentration increases [21]. The larger S value in the fast process indicates that the density of the impurity-induced recombination channels is larger in this process compared with that in the slow process, being consistent with the lower NBE emission intensity, as described above [Fig. 2(c)]. Therefore, both the shorter lifetime and weaker PL intensity of the fast decay is understood by the larger number of impurity-induced recombination channels, and this interpretation is reinforced by the stronger coupling (the larger S value) between the FX and LO phonon at the site with a higher impurity density.

Qualitative consistencies between independent analyses of the PL intensity in the time and energy dependences allow us to further explore the origin of the NBE emission by their quantitative comparisons. Recalling Fig. 3(a), the intensity ratios, I_0/I_1, are estimated to be 0.59 and 0.05 for the fast and

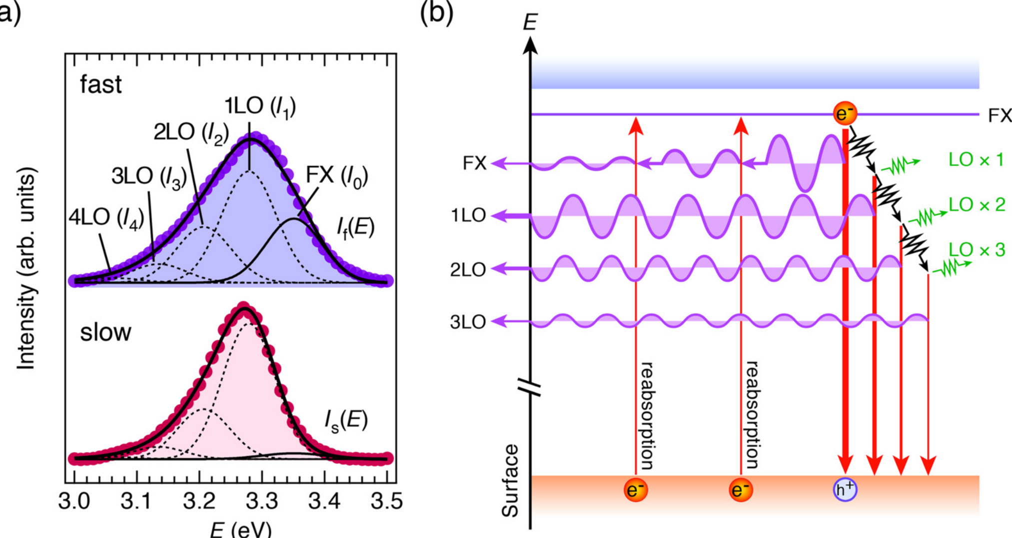

FIG. 3. (a) Fitting results of intensity profiles of $I_f(E)$ and $I_s(E)$. Here, in order to compare the spectral shape, $I_f(E)$ and $I_s(E)$ are normalized to their peak heights. (b) Schematic image of the NBE emission processes that accompany LO phonon excitations and reabsorption processes held inside the crystal. In the recombination processes of electrons in the FX level with holes in the valence band, photons are emitted while exciting some LO phonons. Photons with zero LO phonon excitation are strongly reabsorbed inside the crystal before they escape to the surface. Here, in order to focus on the NBE emissions processes, other recombinations and reabsorption processes that could be induced by impurity/defect states are not illustrated in this image.

slow decays, respectively. These ratios are, however, much smaller than those expected from the relation of $I_0/I_1 = 1/S$ in Eq. (2) (1.00 and 1.35 for the fast and slow decays, respectively). Furthermore, the difference between the observed and expected I_0/I_1 is larger for the slow process than for the fast one. These facts indicate that the intensity of I_0 at the emission site should be largely suppressed when it is emitted from the ZnO sample. This smaller value of I_0 can be understood in terms of the reabsorption process of photons inside the crystal [see Fig. 3(b) and Fig. S6 in the Supplemental Material [22]]. That is, larger reabsorption should proceed for the slow decay than the fast one. The origin of larger reabsorption is probably due to a longer path length of the photons in the crystal (Beer-Lambert law). Thus, a larger suppression of I_0 for the slow decay than for the fast one suggests that the relaxation schemes have taken place at different depths in the crystal, i.e., in the near-surface region for the fast decay process and in the deeper side of the crystal for the slower one. As an alternative reason for the reduction of the I_0 intensity, one may also think that a high carrier concentration may reduce the band gap and promote reabsorption of the FX emission. However, an electronic analysis [27] has revealed the absence of such a high carrier density exceeding 10^{19} cm^{-3} which is required to effectively reduce the band gap [28].

From the above discussion, reduction of the I_0 intensity especially for the slow decay [Fig. 3(a)] suggests that the NBE emission in the high-doped ZnO crystal has a nonuniform spatial distribution: the PL of the fast decay occurs at the surface region, while that of the slow decay originates from deep inside the bulk. The surface-specific recombinations are seemingly originated from a high density of impurities at or near the ZnO surface. Actually, it has been reported that the PL lifetime is shortened by the impurities or vacancies [29] that are preferentially distributed in the depth of several tens of nanometers from a surface [30,31]. Moreover, a previous study showed that the surface defects enhance the FX-LO phonon coupling [32]. Compared to an internal bulk, a surface environmentally induces a high density of impurities and/or vacancies whose density is strongly dependent on surface polishing and cleaning methods. These surface properties consistently explain the prompt decays of the NBE emissions (photoexcited electrons) due to the large number of impurity-induced recombination channels that should distribute over a depth of several tens of nanometers from the surface.

It is of note that the previous time-resolved photoemission spectroscopy (PES) experiment of the high-doped ZnO crystal [27] directly probed the dynamics of photogenerated electron-hole pairs near the surface. Together with the present time-resolved PL experiments, comprehensive major photoreactions and relaxation processes of the photogenerated electron-hole pairs in the ZnO crystal have been elucidated over the time range from ps to μs. This shows that a combination of the time-resolved PL and PES experiments is desired for capturing the whole picture of the electron and hole dynamics in an optoelectronic material. Discussion of the spectral analysis (Fig. 3) indicates that the existence of the two decay components is due to the inhomogeneous crystallinity and infers that the origin of the PL of the fast decay is from the surface region with a higher defect/impurity density than in the bulk. In the low-doped ZnO, only the PL with the single decay time is observed as shown in Fig. 1(c) (see also Fig. S4 in the Supplemental Material [22]). This result suggests that, contrary to the high-doped ZnO crystal, the low-doped one should have homogeneous crystallinity. The origin might be attributed to the sample history, i.e., surface polishing and cleaning methods of the crystals conducted in the companies.

IV. CONCLUSIONS

We conducted time-resolved PL measurements on ZnO crystals to clarify the origin of the NBE emission. Two-relaxation processes, a fast decay process (∼20 ps) and a slow one (∼80 ps), were found in the high-doped ZnO. By deconvoluting the PL spectra using a component for FX and components resulting from coupling with LO phonons, we found that the existence of the two decay components is due to the inhomogeneous crystallinity. These results indicate the necessity to consider spatial distributions of the PL site to understand the FX dynamics. Regarding the application point of view, PL with a fast relaxation time is useful for ultrafast UV light sources [33] and detectors, and that of a slow relaxation time is useful for high-efficiency light-emitting devices and lithographic applications [34]. Our results suggest the feasibility of spatially fine control of the decay time of NBE PL by inducing crystal imperfections with nanofocused ion beams.

In the present research, we introduced the FX-LO phonon coupling model to the spectral analysis of the time-resolved PL data and obtained the dynamical parameters, such as the LO phonon coupling strength and the reabsorption rate of the FX emission, separately for the fast and slow decays. These parameters allow for a deeper understanding of the decay process, i.e., the nonuniform distribution of impurity-induced recombination sites. Our analytical method can be applied to other optoelectronic materials to reveal their origins of the NBE emissions.

ACKNOWLEDGMENTS

We are grateful to T. Sakurai for his help with the Hall measurements. This work was financially supported by Grants-in-Aid for Scientific Research (Grants No. 19H01830 and No. 22H01957) from the Japan Society for the Promotion of Science (JSPS) and by the Murata Science Foundation. The supporting experiments were carried out at SPring-8 BL07LSU of the Synchrotron Radiation Research Organization and at the Institute for Solid State Physics, The University of Tokyo.

[1] Y. F. Chen, D. M. Bagnall, H. Koh, K. Park, K. Hiraga, Z. Zhu, and T. Yao, J. Appl. Phys. **84**, 3912 (1998).
[2] D. C. Look, Mater. Sci. Eng. B **80**, 383 (2001).
[3] S. Lettieri, L. Santamaria Amato, P. Maddalena, E. Comini, C. Baratto, and S. Todros, Nanotechnology **20**, 175706 (2009).
[4] M. Kano, A. Wakamiya, K. Yamanoi, K. Sakai, K. Takeda, M. Cadatal-Raduban, T. Nakazato, T. Shimizu, N. Sarukura, and T. Fukuda, IEEE Trans. Nucl. Sci. **59**, 2290 (2012).
[5] W. Shan, W. Walukiewicz, J. W. Ager, III, K. M. Yu, H. B. Yuan, H. P. Xin, G. Cantwell, and J. J. Song, Appl. Phys. Lett. **86**, 191911 (2005).
[6] A. Teke, Ü. Özgür, S. Doğan, X. Gu, H. Morkoç, B. Nemeth, J. Nause, and H. O. Everitt, Phys. Rev. B **70**, 195207 (2004).
[7] M. R. Wagner, G. Callsen, J. S. Reparaz, J.-H. Schulze, R. Kirste, M. Cobet, I. A. Ostapenko, S. Rodt, C. Nenstiel, M. Kaiser, A. Hoffmann, A. V. Rodina, M. R. Phillips, S. Lautenschläger, S. Eisermann, and B. K. Meyer, Phys. Rev. B **84**, 035313 (2011).
[8] X. T. Zhang, Y. C. Liu, Z. Z. Zhi, J. Y. Zhang, Y. M. Lu, D. Z. Shen, W. Xu, X. W. Fan, and X. G. Kong, J. Lumin. **99**, 149 (2002).
[9] B. Guo, Z. Ye, and K. S. Wong, J. Cryst. Growth **253**, 252 (2003).
[10] T. Koida, S. F. Chichibu, A. Uedono, A. Tsukazaki, M. Kawasaki, T. Sota, Y. Segawa, and H. Koinuma, Appl. Phys. Lett. **82**, 532 (2003).
[11] J. Wilkinson, K. B. Ucer, and R. T. Williams, Radiat. Meas. **38**, 501 (2004).
[12] J. C. Johnson, K. P. Knutsen, H. Yan, M. Law, Y. Zhang, P. Yang, and R. J. Saykally, Nano Lett. **4**, 197 (2004).
[13] J.-C. Deinert, D. Wegkamp, M. Meyer, C. Richter, M. Wolf, and J. Stähler, Phys. Rev. Lett. **113**, 057602 (2014).
[14] K. Yamanoi, T. Shimizu, Y. Furukawa, M. Cadatal-Raduban, T. Nakazato, K. Sakai, M. Tsuboi, R. Nishi, N. Sarukura, M. Tanaka, M. Nishikino, H. Yamatani, K. Nagashima, T. Kimura, T. Fukuda, M. Nagasono, T. Togashi, A. Higashiya, M. Yabashi, T. Ishikawa *et al.*, J. Cryst. Growth **362**, 264 (2013).
[15] Y. G. Wang, S. P. Lau, X. H. Zhang, H. H. Hng, H. W. Lee, S. F. Yu, and B. K. Tay, J. Cryst. Growth **259**, 335 (2003).
[16] T. Komiyama, K. Iwataki, H. Yamaguchi, T. Aoyama, Y. Kashiwaba, and H. Taniguchi, e-J. Surf. Sci. Nanotechnol. **7**, 294 (2009).
[17] A. Shirakov, Z. Burshtein, A. Katzir, E. Frumker, and A. A. Ishaaya, Opt. Express **26**, 11694 (2018).
[18] W.-K. Hong, G. Jo, M. Choe, T. Lee, J. I. Sohn, and M. E. Welland, Appl. Phys. Lett. **94**, 043103 (2009).
[19] J. Kundrotas, A. Čerškus, S. Ašmontas, G. Valušis, M. P. Halsall, E. Johannessen, and P. Harrison, Semicond. Sci. Technol. **22**, 1070 (2007).
[20] Y.-L. Liu, P. Jin, G.-P. Liu, W.-Y. Wang, Z.-Q. Qi, C.-Q. Chen, and Z.-G. Wang, Chin. Phys. B **25**, 087801 (2016).
[21] T. Makino, Y. Segawa, S. Yoshida, A. Tsukazaki, A. Ohtomo, M. Kawasaki, and H. Koinuma, J. Appl. Phys. **98**, 093520 (2005).
[22] See Supplemental Material at http://link.aps.org/supplemental/10.1103/PhysRevMaterials.6.104607 for details about time and energy resolutions in the present experimental setup, characterizations of the shape of the decay curves, fitting results for the PL intensity of the low-doped ZnO crystal, invariance of fitting results, and depth dependent PL spectra.
[23] R. Yukawa, K. Ozawa, S. Yamamoto, H. Iwasawa, K. Shimada, E. F. Schwier, K. Yoshimatsu, H. Kumigashira, H. Namatame, M. Taniguchi, and I. Matsuda, Phys. Rev. B **94**, 165313 (2016).
[24] B. Yan, R. Chen, W. Zhou, J. Zhang, H. Sun, H. Gong, and T. Yu, Nanotechnology **21**, 445706 (2010).
[25] K. Hümmer, Phys. Status Solidi **56**, 249 (1973).
[26] K. Huang and A. Rhys, Proc. R. Soc. London A **204**, 406 (1950).
[27] R. Yukawa, S. Yamamoto, K. Ozawa, M. Emori, M. Ogawa, S. Yamamoto, K. Fujikawa, R. Hobara, S. Kitagawa, H. Daimon,

H. Sakama, and I. Matsuda, Appl. Phys. Lett. **105**, 151602 (2014).
[28] J. G. Lu, S. Fujita, T. Kawaharamura, H. Nishinaka, Y. Kamada, T. Ohshima, Z. Z. Ye, Y. J. Zeng, Y. Z. Zhang, L. P. Zhu, H. P. He, and B. H. Zhao, J. Appl. Phys. **101**, 083705 (2007).
[29] M. A. M. Versteegh, T. Kuis, H. T. C. Stoof, and J. I. Dijkhuis, Phys. Rev. B **84**, 035207 (2011).
[30] K. Vanheusden, W. L. Warren, C. H. Seager, D. R. Tallant, J. A. Voigt, and B. E. Gnade, J. Appl. Phys. **79**, 7983 (1996).
[31] I. Shalish, H. Temkin, and V. Narayanamurti, Phys. Rev. B **69**, 245401 (2004).
[32] C. H. Ahn, S. K. Mohanta, N. E. Lee, and H. K. Cho, Appl. Phys. Lett. **94**, 261904 (2009).
[33] M. Kano, A. Wakamiya, K. Sakai, K. Yamanoi, M. Cadatal-Raduban, T. Nakazato, T. Shimizu, N. Sarukura, D. Ehrentraut, and T. Fukuda, J. Cryst. Growth **318**, 788 (2011).
[34] M. Tanaka, M. Nishikino, H. Yamatani, K. Nagashima, T. Kimura, Y. Furukawa, H. Murakami, S. Saito, N. Sarukura, H. Nishimura, K. Mima, Y. Kagamitani, D. Ehrentraut, and T. Fukuda, Appl. Phys. Lett. **91**, 231117 (2007).